Journal of Computer Assisted Tomography
24(6):949–957

High-Resolution MR Venography at 3.0 Tesla

Jürgen R. Reichenbach, Markus Barth, E. Mark Haacke, Markus Klarhöfer, Werner A. Kaiser, and Ewald Moser

Purpose: The aim of this study was to investigate the visualization of small venous vessels in the normal human brain at a field strength of 3 Tesla.

Methods: T2*-weighted, three-dimensional gradient-echo images were acquired by exploiting the magnetic susceptibility difference between oxygenated and deoxygenated hemoglobin in the vasculature and microvasculature. The spatial resolution was $0.5 \times 0.5 \times 1$ mm^3, and sequence parameters were varied to obtain good vessel delineation. Improved visibility of venous vessels was obtained by creating phase mask images from the magnetic resonance phase images and multiplying these by the magnitude images. Venograms were created by performing a minimum intensity projection over targeted volumes.

Results: Highly detailed visualization of venous structures deep in the brain and in the superficial cortical areas were obtained without administration of an exogenous contrast agent; compared with similar studies performed at 1.5 T, the echo time could be reduced from typically 40–50 ms to 17–28 ms.

Conclusion: Imaging at high-field strength offers the possibility of improved resolution and the delineation of smaller vessels compared with lower field strengths.

Key Words: Magnetic resonance imaging–Blood oxygen level dependent (BOLD)–3.0 Tesla–Venogram–Phase–Susceptibility.

INTRODUCTION

Imaging the venous system of the human brain noninvasively may be of great importance in the assessment and evaluation of vasculature and brain tissue both in the normal and diseased state. From a clinical point of view it is often useful to be able to differentiate between arteries and veins because the latter can play an important role in the pathophysiology of certain lesions. The vascular structure in the brain is organized in a rather complicated and intricate pattern (1). The smaller vessel sizes range in diameter from several microns for capillaries to several tens of microns for venules, precapillary sphincters, and arterioles to several 100 μm for small pial arteries and veins (2). The mean flow velocity changes are inversely proportional to the cross-sectional area. In pial vessels, the mean flow velocity ranges from several mm/s to a few cm/s, whereas in the capillaries it is only on the order of 0.5 to 3 mm/s (3). However, due to the usually slow flow of blood in small vessels, they are difficult to detect with conventional magnetic resonance (MR) methods, such as time-of-flight (TOF) or phase contrast angiography (PCA) (4). Although several different MR methods exist for the evaluation of venous vasculature (5–8), most of the recent advances have been made in the development of techniques assessing the arterial system; high-resolution MR techniques to image the venous system of the brain are not as commonly available.

Recently, a high-resolution, three-dimensional (3D) gradient echo imaging technique has been proposed that makes it possible to visualize uniquely venous structures at 1.5 Tesla (9,10). The underlying contrast mechanism is associated with the magnetic susceptibility difference between oxygenated and deoxygenated hemoglobin in the vasculature and microvasculature. While the oxygenated hemoglobin iron atom is diamagnetic, the deoxygenated iron atom containing four unpaired electrons is paramagnetic. Thus a change or a difference in the oxygenation state of arterial and venous blood manifests itself as a change or difference in the bulk magnetic

Institut für Diagnostische und Interventionelle Radiologie (J. R. Reichenbach, W. A. Kaiser), Friedrich-Schiller-Universität, Jena, Germany, Section of Osteology (M. Barth), Department of Radiodiagnostics, University of Vienna, Vienna, Austria, The Magnetic Resonance Imaging Institute for Biomedical Research (E. Mark Haacke), St. Louis, MO, U.S.A., and Arbeitsgruppe-NMR (M. Klarhöfer, E. Moser), Institut für Medizinische Physik, Universität Wien, Vienna, Austria. Address correspondence and reprint requests to Dr. J. R. Reichenbach, Institut für Diagnostische und Interventionelle Radiologie, Abteilung Magnetresonanztomographie, Klinikum der Friedrich-Schiller-Universität Jena, Philosophenweg 3, 07743 Jena, Germany. E-mail: rbach@mrt.uni-jena.de

susceptibility of the blood. Consequently, this blood oxygenation level dependent (BOLD), susceptibility-based contrast-to-noise ratio is expected to be higher at higher field strengths (11,12). The recent development of high-field whole-body scanners up to 8 Tesla (13) has made it possible to expand these imaging applications for functional brain imaging, spectroscopy, and brain imaging with high anatomic resolution, while exploiting the inherently higher signal-to-noise ratio compared with conventional systems. The biologic tissue signal-to-noise ratio (SNR) scales with the field strength B_0 of the instrument magnet, to at least the first power. Higher SNR, in turn, translates into better temporal resolution, or better spatial resolution, or some combination of the two. The aim of this study was to investigate the visualization of venous vessels in the normal human brain at a high-field strength of 3 Tesla using high resolution, gradient-echo MR imaging.

THEORY

The technique for visualizing the venous system is based on the BOLD effect, which exploits the fact that paramagnetic deoxyhemoglobin causes a local magnetic field inhomogeneity, resulting in both a reduction of T2* and a phase difference between the venous vessel and its surroundings (11,14). Both effects depend on the regional concentration of deoxyhemoglobin and the oxygen saturation of blood.

The first effect leads to signal loss due to changes of T2* relaxation time with changing blood oxygen saturation (15–18). In veins, the blood oxygenation is smaller than that in arteries, which causes a lower signal due to an increase of the transverse relaxation rate constant $R_2^*(Y)$. The signal evolution of blood as a function of echo time can be written as

$$S(TE) = S_0 \cdot \exp(-R_2^*(Y) \cdot TE) \quad [1]$$

where $R_2^*(Y)$ can be approximated by a polynomial expression to second order as a function of Y at 1.5 Tesla (18). With a higher field strength, T2 relaxation times shorten substantially, leading to increased signal reduction of venous blood due to the net dephasing of proton spins moving in and around the red blood cells.

The second effect is due to bulk magnetic susceptibility within the venous vessel, which causes an average frequency shift for all protons inside the vessel (19). The spin precession phase angle ϕ of the venous blood signal due to the bulk magnetic susceptibility inside the vessel can be written as

$$\phi(TE) = \gamma \cdot \Delta B \cdot TE \quad [2]$$

where γ is the magnetogyric ratio for protons (2.678×10^8 *rad / s / T*), ΔB the field difference between blood and the surrounding tissue, and TE the echo time. For a vessel modeled as an infinitely long straight cylinder (i.e., a straight vein with a diameter much smaller than its length), ΔB can be written as (20)

$$\Delta B = 2 \cdot \pi \cdot \chi_{do} \cdot B_0 \cdot \left(\cos^2 \theta - \frac{1}{3}\right) \cdot (1 - Y) \cdot Hct \quad [3]$$

where $\chi_{do} = 0.18 \cdot 10^{-6}$ is the susceptibility difference between fully deoxygenated and fully oxygenated blood (21), B_0 the external field strength, Y is the fractional oxygen saturation of the blood in the vessel, and *Hct* is the average volume fraction of hematocrit in blood. θ represents the angle between the blood vessel and the static field B_0. In healthy subjects the value for *Hct* is approximately 0.40 (22).

For instance, setting $B_0 = 3$ T, $Y = 0.54$ (23), and $Hct = 0.40$ in Eq. [3], and assuming a vessel is oriented parallel to the magnetic field ($\theta = 0°$) yields $\phi \approx 35 \cdot \pi \cdot$ TE. Using TE $\approx$ 28 ms results in $\phi = \pi$, and the signal of the venous blood is predicted to oppose that of the background tissue. This leads to maximum signal cancellation for a vein with a diameter less than the pixel size Δx. If $\theta \neq 0°$, there exists an additional extravascular field surrounding the vessel besides the intravascular field (Eq. [3]), which will also cause signal cancellation due to the induced magnetic field microgradients in the perivascular space (23,24). In gradient echo imaging the signal loss caused by intravascular phase changes, and the cancellation of the venous blood signal with surrounding parenchyma, show large effects, which make it possible to visualize even small, subvoxel-size vessels due to these partial volume effects (23). High spatial resolution increases the venous blood volume fraction within a voxel and leads to better vascular visualization (25).

MATERIALS AND METHODS

High-resolution, T2*-weighted, single-echo images were acquired on a 3 T system (Medspec 30/80 Avance, Bruker Medical, Ettlingen, Germany) with a 3D, first-order velocity compensated gradient echo sequence using a quadrature, transmit/receive birdcage head coil. The maximum available gradient strength was 19 mT/m with a rise-time of 150 μs. The gradient motion rephasing was implemented in all three directions to ensure that spins moving with constant velocity have zero net phase gain at echo time. Automated shimming of all first- and second-order shim coils was done, typically resulting in a 20–30 Hz line-width of the water resonance from the entire volume of the head.

Three healthy volunteers (ages 25–37 years, 1 male and 2 female) participated in the investigation. Informed consent was obtained from each subject following the guidelines of the institutional review board. One patient with a venous angioma was investigated using the high resolution 3D scan.

Sequence parameters were slightly varied for the volunteer studies with typical values ranging from TR = 46–51 ms, TE = 17–28 ms, α = 16–40°, FOV = 192 × 256 mm^2 or 256 × 256 mm^2, and matrix size = 384 × 512 or 512 × 512. Usually, 48 to 64 partitions were

acquired with a partition thickness of 1 mm yielding a typical voxel size of 0.25 mm^3. Depending on the specific parameter settings the acquisition time ranged between 15 to 20 minutes. Both magnitude and phase images were reconstructed from the raw data. To remove incidental phase variations in the images due to static magnetic field inhomogeneity effects, a homodyne demodulation reference derived from the raw data images was used (26,27). A symmetric 2D Hamming window was applied to the 2D k-space raw data for each partition with the filter coefficients $w(n)$ computed according to the formula:

$$w(n) = 0.54 + 0.46 \cdot \cos\left(\frac{\pi \cdot n}{N}\right) \qquad -N \leq n < N \quad [4]$$

The filter size was set to 32 × 32, which was found to yield homogeneous phase images sufficiently while still preserving the spatially localized susceptibility induced phase changes due to the presence of venous blood. The low-pass filtered reconstructed phase images were subtracted from the original phase images using complex division. The assessment of the filter effect was based on visual inspection of the resulting phase images. Although filter sizes of 16 × 16 and 64 × 64 were also tested, the best results were obtained with the chosen size in our small study group. With the smaller filter size, the slowly varying phase variations were not always removed completely, whereas with the larger filter size, small details in the phase images started to disappear. Similar findings were reported in Ref. 27. Image processing was done with IDL (Research Systems, Boulder, CO, U.S.A.).

Magnitude images were segmented to separate brain parenchyma from the skull and background. Improved visibility of the venous vessels was obtained by designing phase mask filter images from the reconstructed corrected phase images and multiplying these filter images with the corresponding magnitude images several times (9,10). The postprocessing algorithm created these multiplied images automatically where the number of multiplications ranged from three to nine. The motivation for applying a phase mask filter was due to paramagnetic structures running parallel to the magnetic field, such as veins containing deoxygenated blood, which have a higher resonance frequency (i.e., they experience a stronger local magnetic field at the proton sites), compared with the surrounding parenchyma and cerebrospinal fluid. The phase contrast of venous vessels thus appears dark on phase images. The phase mask was created by setting phase values above a threshold of 0° to unity, whereas all phase values below the threshold and larger than $-\pi$ were linearly scaled between zero and unity with zero corresponding to $-\pi$ (see Fig. 1). Several venograms were created by performing a minimum intensity projection (mIP) over targeted volumes of the differently multiplied magnitude images of typically 10 to 15 partitions (9,10). The venogram showing the best appearance and conspicuity on visual inspection was chosen for display. Therefore, the number of multiplications used in creating the venograms differs between volunteers.

In addition, a conventional 3D TOF, multislab, gradient-echo sequence was also acquired in two cases. The sequence parameters were TR = 40 ms, TE = 9 ms, α = 40°, FOV = 256 mm. The echo was asymmetrically sampled with the echo center at 30% of the acquisition window. The in-plane resolution was 1.0 × 1.0 mm^2. Typically, 3 overlapping slabs each consisting of 32 partitions with a partition thickness of 1 mm were acquired in transverse orientation and were centered around the high ventricular level covering approximately the same brain volume as the venography scan. The scans were acquired with a TONE (tilted optimized nonsaturating excitation) pulse to reduce inflow saturation (28). Maximum intensity projections (MIP) were performed over the same targeted volumes as the venograms.

RESULTS

Figure 2A displays the original reconstructed phase image of a single section of the 3D complex raw data set containing the low frequency, spatially varying incidental phase modulations due to static field inhomogeneities and background gradients. Figures 2B and 2C show the low-resolution filtered phase image with filter size 32 × 32 used for correction and the final corrected phase image, respectively. Note that the fine spatial details due to the susceptibility induced phase changes of the venous vessels are preserved in Figure 2C, whereas the overall phase image appears rather homogeneous.

Figure 3 shows an original single magnitude partition,

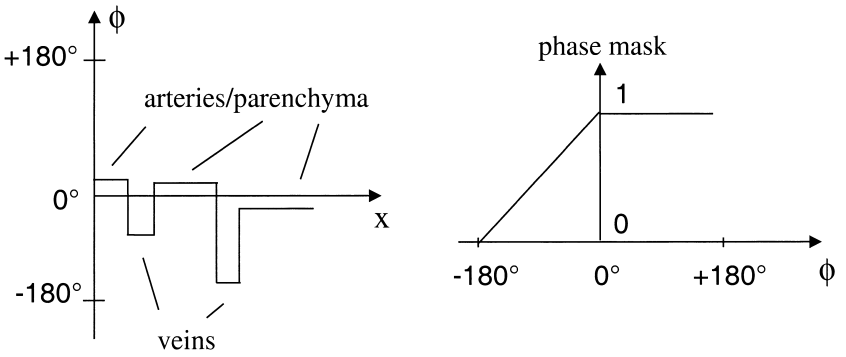

FIG. 1. Schematics illustrating the principle of the phase mask filter. Due to the more paramagnetic susceptibility of venous vessels, the phase appears dark with negative values in the phase images, whereas parenchyma, cerebrospinal fluid, and arteries will show both small positive and negative phase values distributed more closely around zero.

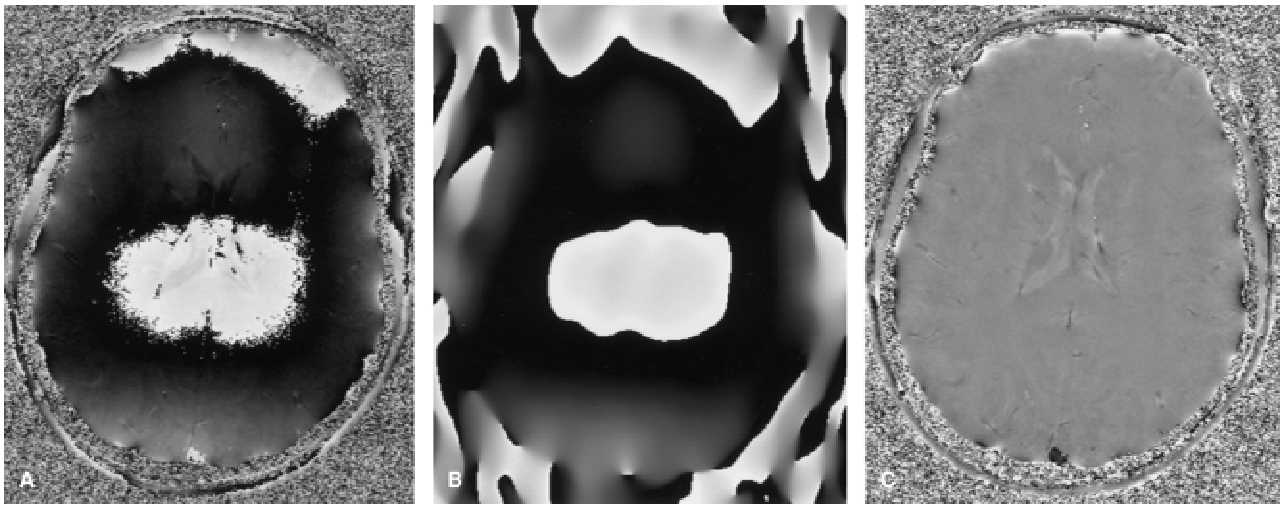

FIG. 2. A: Original phase image of a single partition of the 3D data set. **B:** Reconstructed low resolution, 2D Hamming window filtered phase image. **C:** Corrected phase image after phase subtraction. Sequence parameters: TR = 46 ms, TE = 17 ms, $\alpha = 16°$, 81 Hz/pixel, FOV = 256 × 256 mm^2, matrix = 512 × 512, 48 partitions, 1 mm thickness, TA = 18:43 min.

the same magnitude image after nine multiplications by the phase mask filter image, as well as the corresponding venogram obtained after performing an mIP operation of over 17 mm. Figure 3C illustrates the rich and complex venous structure deep in the brain as well as in the cortical areas. Note also the differentiation between gray matter and white matter in the venogram. Compared with similar studies performed at 1.5 T (9,10), the echo time has been reduced from 40 to 50 ms to 28 ms in this case.

Figure 4 compares the influence of echo time TE on the projected venograms. Each mIP corresponds to the same targeted volume of 15 mm. The phase mask filter was applied three times in each case. With longer TE, the contrast between brain parenchyma and veins becomes sharper, and the venous vascular system is delineated in more detail and appears with more conspicuity, as can be seen in the enlarged regions of the venograms (Figs. 4C and D). To compare the venograms with an MR angiogram, Fig. 4E contains the MIP image of the 3D TOF MRA projected over the same volume. Because no presaturation pulses were applied and a relatively small slab was used, the image not only shows arterial vessels but also fast flowing venous vessels, such as the superior sagittal sinus. Small vessels, however, are not visualized due to saturation effects.

Figure 5 shows a venogram in the sagittal orientation. The lateral projection was calculated over 17 mm. To avoid image artifacts due to pulsatile motion of the fast flowing arterial blood, the vascular signal of the internal carotid and the vertebral arteries was suppressed by applying a presaturation pulse outside the imaging volume. Flowing arterial spins enter the volume with virtually

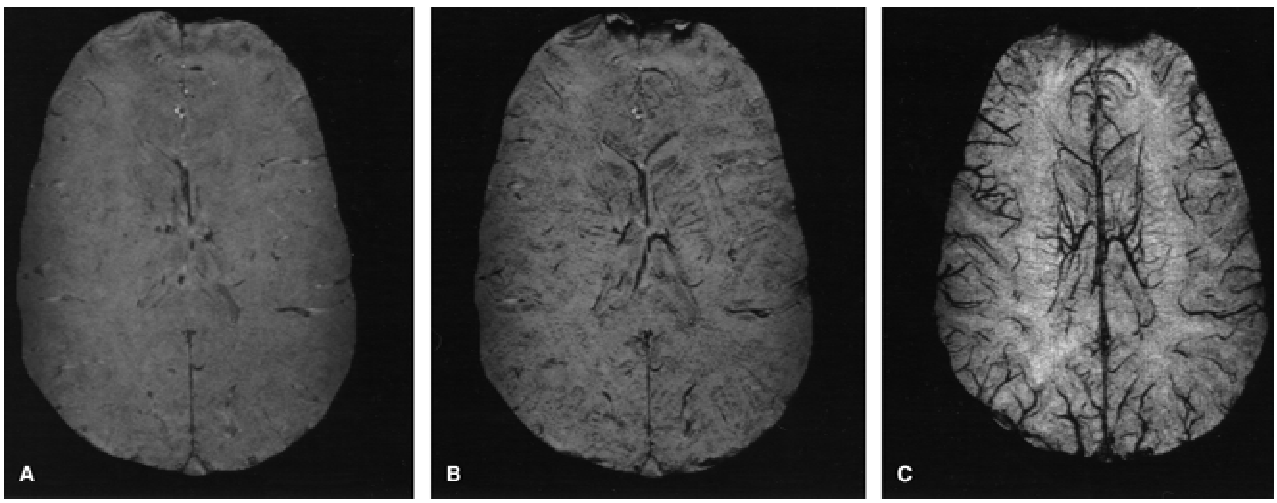

FIG. 3. A: Transverse MR image of the brain at 3.0 Tesla. Single-section acquired with the following sequence parameters: TR/TE/α = 51 ms/28 ms/40°, FOV = 192 × 256 mm^2, matrix = 384 × 512, 48 sections, partition thickness 1mm. **B:** Magnitude image after nine multiplications with the phase mask filter. **C:** The corresponding minimum intensity projection calculated over 17 sections.

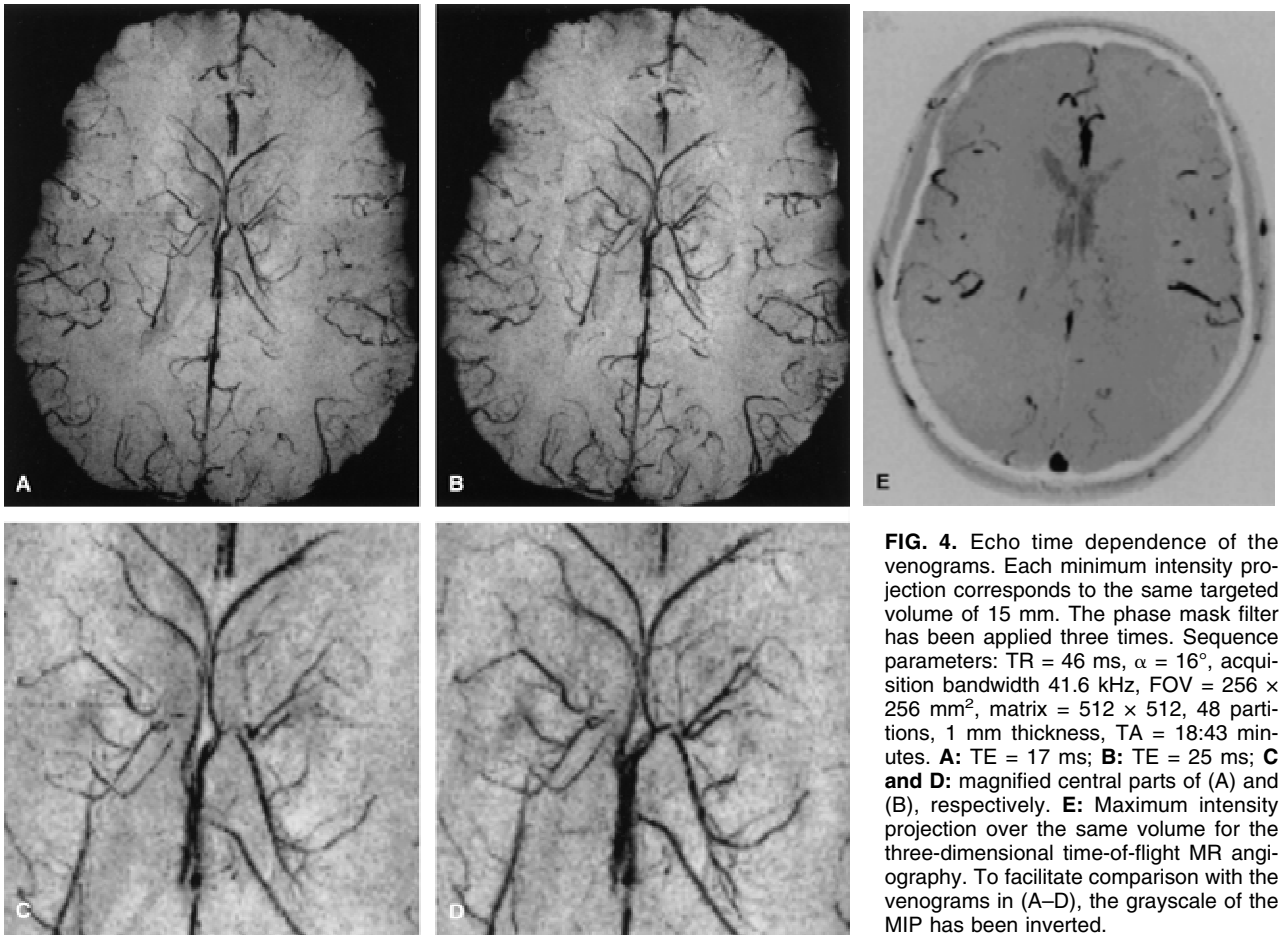

FIG. 4. Echo time dependence of the venograms. Each minimum intensity projection corresponds to the same targeted volume of 15 mm. The phase mask filter has been applied three times. Sequence parameters: TR = 46 ms, α = 16°, acquisition bandwidth 41.6 kHz, FOV = 256 × 256 mm^2, matrix = 512 × 512, 48 partitions, 1 mm thickness, TA = 18:43 minutes. **A:** TE = 17 ms; **B:** TE = 25 ms; **C and D:** magnified central parts of (A) and (B), respectively. **E:** Maximum intensity projection over the same volume for the three-dimensional time-of-flight MR angiography. To facilitate comparison with the venograms in (A–D), the grayscale of the MIP has been inverted.

complete signal cancellation, and are consequently picked up by the mIP operation. Although major arteries with fast flow also appear dark in this case, these vessels are usually easily identified and normally do not create a real problem in interpreting the images. Note, however, the delineation of the detailed venous vascular network, especially in the occipital part of the brain.

Venograms in transverse and reformatted coronal orientation are shown in Figure 6, together with the capillary and venous phase of an intraarterial digital subtraction angiography (DSA) for a patient with a venous angioma. The venogram in Figure 6A clearly demonstrates the venous drainage of the arteriovenous malformation (AVM) via the right anterior septal vein. The coronal venogram (Fig. 6B) shows the lesion in a similar orientation as the catheter angiograms (Figs. 6C and D).

DISCUSSION

The ability to visualize the venous system in vivo with high spatial resolution may have important ramifications for understanding brain function and vascular morphology. MR venography makes it possible to provide information about the geometric parameters of the venous vascular network. Although these parameters do not always correlate with the intensity of the blood flow in a particular region of the brain, they characterize the state of the regional blood supply and drainage as well as of the local blood volume to some extent. Imaging at high-field strengths offers the possibility of improved resolution due to higher SNR and, thus, delineation of even smaller vessels compared with lower fields. As demonstrated here, MR venography has the potential to rival the resolution known from conventional DSA studies. This, in turn, may help to assess the vascular extent of brain lesions, such as highly vascularized tumors (29), arteriovenous malformations (30), or venous angiomas (31), even without application of a contrast agent. Typically, MR venography is performed without administration of a contrast agent using 2D TOF or 3D phase contrast angiography (PCA) techniques (32). However, it has been reported in the literature that for the visualization of venous vessels, especially those with small caliber, administration of contrast agent may help to highlight these vessels and improve the vascular conspicuity (7,8,33,34). In contrast, the technique described in this paper does not require contrast enhancement or subtraction of an unenhanced from an enhanced data set to better portray small venous structures.

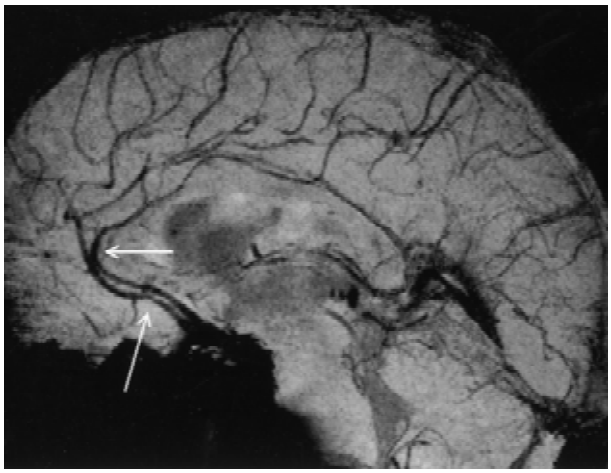

FIG. 5. Sagittal venogram (lateral projection). Sequence parameters: TR/TE = 49 ms/17 ms, FOV = 256 × 256 mm^2, matrix = 512 × 512, 48 sections, thickness 1mm. The projection was calculated over 17 mm, and the phase mask filter was applied twice. Due to the application of a presaturation pulse outside the imaging volume, the anterior cerebral arteries are saturated (see white arrows) and appear dark in this image (see text).

The basic mechanism of the method relies on the signal cancellation between parenchyma and venous blood. If a voxel contains a small vein with a certain blood volume fraction that corresponds to an MR signal fraction of λ and brain tissue with a signal fraction of 1-λ, the phase difference between the two materials caused by the different local Larmor frequencies will increase with TE and will lead to a smaller resulting voxel signal. The maximum magnitude difference is 2λ, if we neglect T2* relaxation. If the final signal is larger than the noise level in the image, the venous vessels can be inferred indirectly from this signal drop. The image processing that is performed helps to highlight the veins (Fig. 1). Our reason for changing the number of times that the mask is applied was to tailor and optimize the final venograms for each individual case, which can be done very easily with the automated algorithm described in the Methods section, followed by visual inspection. As has been described in Ref. 10, for a field strength of 1.5 T best results using this approach were obtained with 3–5 multiplications prior to the mIP operation. With the exception of one case, in which for unknown reasons the num-

FIG. 6. A 63-year-old patient with a venous angioma located frontally on the right side. **A:** High resolution MR venogram in transverse orientation showing the collecting veins and the draining anterior septal vein of the malformation (TR/TE = 65 ms/28 ms, TH = 2 mm, 32 partitions, FOV = 192 × 256 mm^2, matrix = 384 × 512, mIP = 8 mm, phase mask ×4). **B:** Reformatted venogram in coronal orientation and centered at the lesion shown in (A). The projection was performed over six slices. The venogram appears inferior compared with (A) due to the voxel dimensions not being isotropic. **C:** Capillary phase of selective intraarterial DSA of the right internal carotid artery showing the feeding vessels of the arteriovenous malformation (arrow). **D:** Venous phase of the DSA demonstrating the venous drainage (arrows), which is also seen on the MR venograms in (A) and (B).

ber of multiplications was quite high (n = 9), these quoted numbers lead also to very convincing results at 3 T. In particular, as seen in Figures 3 and 4, application of the postprocessing results in a prominent visualization of multiple small cortical veins and small deep medullary veins. By comparison with an anatomic radiographic image acquired on a postmortem sample (1), we can infer the size of the smallest venous vessels as seen on Figure 4, which we estimate to be on the order of 100–200 μm. Unfortunately, there are no vessel sizes or projected volumes specified in the radiographic atlas of the venous anatomy. However, the main point here is that the smallest visualized vessels in the MR venogram can be much smaller than a pixel element.

One surprising result, however, is the fact that small veins, such as the deep medullary veins, running perpendicular to the magnetic field are still better delineated by using the phase mask filter. Although Eq. [3] predicts a change in sign in the offset field ΔB when passing the "magic angle" of 54.74°, which causes a value of unity in the phase mask filter, these veins are better defined after application of the filter mask than prior to it (see Fig. 3). Similar findings were reported by Lin et al. (35). One explanation may be that Eq. [3] only describes the intravascular aspect of the BOLD effect and does not consider any extravascular sources to the observed signal. As is well known, there exists also an extravascular field offset with an angular dependence outside the vein, if the vessel is not oriented parallel to the external field (23). This leads to a local increase of signal loss, and for vessels smaller than a voxel it may explain the observed phase as well. Furthermore, Eq. [3] is based on the assumption of an infinitely extended cylinder, which may be violated under real physiological conditions. Consequently, full modeling of the detailed vascular conformation would be required to predict both intravascular and extravascular contributions to the phase and signal behavior around small venous vessels.

Further remarks should be made about several aspects of the technique. The carefully calculated gradient design for flow compensation may not yield zero phase at the echo center due to eddy currents and cumulative build-up of other gradient-induced effects with the long echo times used in this study. This nonzero remnant phase value may represent a problem in case of fast or pulsatile flowing blood, such as major cerebral arteries, because the dephased signal will be falsely interpreted as a susceptibility induced phase effect and may be picked up by the data processing. These vessels, however, are usually easily identified and do not represent a real problem in interpreting the images.

Although the BOLD-contrast mechanism is directly related to the strength of the main magnetic field (11,36), susceptibility-based signal loss and severe image distortion caused by air–tissue interfaces or other sources of local field inhomogeneity are much more severe at higher fields. Consequently, shimming is very important to obtain useful images. Application of this method, however, may be difficult in areas with B_0 inhomogeneity and may be restricted to anatomic brain regions, avoiding large static field inhomogeneities caused by susceptibility differences, such as regions near the paranasal sinuses and skull base; although in theory, it is still possible to overcome these limitations, at least partially and at the expense of time, by using higher spatial resolution (37). Another possibility to overcome the signal loss due to strong local magnetic field gradients around air and tissue interfaces is to use, for example, a multigradient echo with magnetic susceptibility inhomogeneity compensation method (MGESIC) (38).

An elegant way to reduce the increased sensitivity to susceptibility artifacts caused by the relatively long TE and high field strength is to use a T1-reducing contrast agent to obtain venograms with shorter TE and shorter TR. Recently, Lin et al. (35) have demonstrated the utility of this approach while still maintaining the visibility of cerebral venous vessels at a field strength of 1.5 T. By using a T1 shortening agent, the blood signal fraction of the veins becomes larger at a given echo time, which leads to an enhanced cancellation effect between venous blood and background tissue and, thus, to a better delineation of the venous network. With a double-dose injection, the authors were able to reduce TE from 40 to 25 ms in their study. Using the same method at 3 T should allow for similar reduction of TE from 28 to 18 ms while still maintaining the visibility of the vessels. One important point to consider, however, relates to the fact that contrast administration induces increased T2* effects at higher field strength. Consequently, one has to optimize the amount of contrast agent to avoid severe T2*-shortening while still taking advantage of the T1-reducing effect of the agent. This should be investigated in future clinical studies.

We found that flip angles larger than the calculated Ernst angles for gray ($\alpha = 15°$) and white ($\alpha = 19°$) matter, using the TR quoted above and T1 values of 1,331 ms and 832 ms for GM and WM, respectively (39), resulted in a better GM-to-WM contrast in the projected venograms (see for example Figure 3C). A similar observation of improved contrast between gray and white matter was made by Wansapura et al. (39) when using higher flip angles than the calculated Ernst angles. Thus the flip angle can be used as an adjustable parameter, which influences the final degree of contrast between GM, WM, and the delineation of the venous vessels in the reconstructed venograms.

In conclusion, we demonstrated that high-resolution venography at a field strength of 3 T is possible and allows shorter echo times with respect to maximum signal cancellation (28 ms versus 50 ms) compared with 1.5 T. This makes it possible to improve the spatial resolution, increase the spatial coverage, or shorten the acquisition time, which, in turn, makes potential patient examinations more feasible in assessing venous vasculature in a normal or diseased state with high resolution. We have obtained a good overall representation of cerebral venous structures with echo times as short as 17 ms without using an exogenous contrast agent in volunteers

and a patient. The high spatial resolution was used with a voxel volume of $0.5 \times 0.5 \times 1$ mm^3, compared with typical voxel sizes of $0.5 \times 1 \times 2$ mm^3 or $1 \times 1 \times 2$ mm^3 routinely applied at 1.5 T (9,10,35).

The SNR is directly proportional to the voxel volume. Assuming that all sequence and tissue parameters are the same at both field strengths implies a reduced SNR by a factor of 4 and 8 at 3 T, respectively, which is partly compensated by the linear increase of the SNR with the magnetic field strength (40,41). The NMR signal is proportional to both the degree of proton magnetization and to the rate of Larmor precession. Thus the signal strength increases in proportion to the square of the magnetic field strength. Unfortunately, however, the thermal noise originating in the patient increases linearly with field strength. These opposing effects suggest that the SNR will increase in an approximately linear fashion with field strength. SNR is also improved by the increased number of phase-encoding steps, which results in an additional factor of $\sqrt{2}$ with the higher resolution used here. Furthermore, SNR is proportional to instrument-related factors, such as the sensitivity of the RF coils and the measured magnetization, which, in turn, is a complex function of acquisition parameters (TR, TE, α) and intrinsic tissue parameters (T1, T2). From a practical point of view it appears that the SNR in the present high resolution study, though possibly lower than that at 1.5 T by a factor of $\sqrt{2}$ or even less, suffices to produce high quality venograms, as is exemplified in Figures 3 to 6.

In summary, high resolution BOLD venographic imaging offers the ability to image venous blood in its deoxygenated state for vessels on the order of 100 to 200 microns. We believe that the technique is superior in resolving small venous vessels compared with 2D TOF venography or to contrast-enhanced MR venography studies. To the best of our knowledge, we are not aware of a MR study performed at 3 T that shows the deep venous system in the brain in such detail. Recent work published by the Ohio Group also has shown venous vessels with superb resolution; however, this study was performed at 8 T (42). As has been demonstrated, the technique appears promising in the assessment of intracranial vascular-related lesions, such as arteriovenous malformation or venous angioma. Further studies at high-field strengths, especially with an optimized and tailored administration of a T1-shortening contrast agent to reduce TE even further, would be valuable in evaluating the full clinical potential of this method in vascular-related diseases associated with increased blood flow, increased venous drainage, or in evaluating the vascularity of tumors.

REFERENCES

1. Salamon G, Huang YP. *Radiologic Anatomy of the Bain*. Berlin: Springer-Verlag, 1976.
2. Berne RM, Levy MN. The Circuitry. In: Berne RM, Levy MN, eds. *Physiology.* 2nd ed. St. Louis: Mosby, 1988:395–97.
3. Pawlik G, Rackl A, Bing RJ. Quantitative capillary topography and blood flow in the cerebral cortex of cats: an in-vivo microscopic study. *Brain Res* 1981;208:35–58.
4. Potchen EJ, Haacke EM, Siebert JE, et al. *Magnetic Resonance Angiography*. St. Louis: Mosby, 1993.
5. Cho ZH, Ro YM, Lim TH. NMR venography using the susceptibility effect produced by deoxyhemoglobin. *Magn Reson Med* 1992;28:25–38.
6. Ozsvath RR, Casey SO, Lustrin ES, et al. Cerebral venography: comparison of CT and MR projection venography. *Am J Roentgenol* 1997;169:699–707.
7. Stevenson J, Knopp EA, Litt AW. MP-RAGE Subtraction venography: A new technique. *J Magn Reson Imaging* 1995;5:239–41.
8. Ikawa F, Sumida M, Uozumi T, et al.. Demonstration of the venous systems with gadolinium-enhanced three-dimensional phase-contrast MR venography. *Neurosurg Rev* 1995;18:101–7.
9. Reichenbach JR, Venkatesan R, Schillinger DJ, et al. Small vessels in the human brain: MR venography with deoxyhemoglobin as an intrinsic contrast agent. *Radiology* 1997;204::272–7.
10. Reichenbach JR, Essig M, Haacke EM, et al. High-resolution venography of the brain using magnetic resonance imaging. *MAGMA* 1998;6:62–9.
11. Ogawa S, Lee TM, Nayak AS, et al. Oxygenation-sensitive contrast in magnetic resonance image of rodent brain at high magnetic fields. *Magn Reson Med* 1990;14:68–78.
12. Turner R, Jezzard P, Wen H, et al. Functional mapping of the human visual cortex at 4 and 1.5 Tesla using deoxygenation contrast EPI. *Magn Reson Med* 1993;29:277–9.
13. Robitaille PML, Warner R, Jagadeesh J, et al. Design and assembly of an 8 Tesla whole-body MR scanner. *J Comput Assist Tomogr* 1999;23:808–21.
14. Hoogenraad FGC, Reichenbach JR, Haacke EM, et al. In vivo measurement of changes in venous blood-oxygenation with high resolution functional MRI at 0.95 Tesla by measuring changes in susceptibility and velocity. *Magn Reson Med* 1998;39:97–107.
15. Thulborn KR, Waterton JC, Matthews PM, et al. Oxygenation dependence of the transverse relaxation time of water protons in whole blood at high field. *Biochim Biophys Acta* 1982;714: 265–70.
16. Chien D, Levin DL, Anderson CM. MR gradient echo imaging of intravascular blood oxygenation: T2* determination in the presence of flow. *Magn Reson Med* 1994;32:540–5.
17. Barth M, Moser E. Proton NMR relaxation times of human blood samples at 1.5 T and implications for functional MRI. *Cell Mol Biol* 1997;43:783–91.
18. Li D, Wang Y, Waight D. Blood oxygen saturation assessment in vivo using T2* estimation. *Magn Reson Med* 1998;39:685–90.
19. Springer CS. Physicochemical principles influencing magnetopharmaceuticals. In: Gillies RJ, ed. *NMR in Physiology and Biomedicine*. New York: Academic Press, 1994:75–99.
20. Chu SCK, Xu Y, Balschi JA, et al. Bulk magnetic susceptibility shifts in NMR studies of compartmentalized samples: use of paramagnetic reagents. *Magn Reson Med* 1990;13:239–62.
21. Weisskoff RM, Kiihne S. MRI susceptometry: image-based measurement of absolute susceptibility of MR contrast agents and human blood. *Magn Reson Med* 1992;24:375–83.
22. Guyton AC. *Textbook of Medical Physiology*. 7th ed. Philadelphia: WB Saunders, 1986:206.
23. Haacke EM, Lai S, Yablonskiy DA, et al. In vivo validation of the BOLD mechanism: a review of signal changes in gradient echo functional MRI in the presence of flow. *Int J Imaging Syst Technol* 1995;6:153–63.
24. Yablonskiy DA, Haacke EM. Theory of NMR signal behavior in magnetically inhomogeneous tissues: the static dephasing regime. *Magn Reson Med* 1994;32:749–63.
25. Venkatesan R, Haacke EM. Role of high resolution in MR imaging: applications to MR angiography, intracranial T1-weighted imaging and image interpolation. *Int J Imaging Syst Technol* 1997;8:529–43.
26. Noll DC, Nishimura DG, Macovski A. Homodyne detection in magnetic resonance imaging. *IEEE Trans Med Imaging* 1991;MI-10:154–63.
27. Yu Y, Wang Y, Haacke EM, et al. Static field inhomogeneity

correction using a 3D high pass filter. *Proc Intl Soc Mag Reson Med* 1999;7:180.
28. Purdy D, Cadena G, Laub G. The design of variable tip angle slab selection (TONE) pulses for improved 3D MR angiography. In: *Proc SMRM.* 11th Annual Meeting, Berlin 1992, p. 882.
29. Haacke EM, Lin W, Mukherjee P, et al. Application of 3D gradient echo imaging in observing lesion vascularity. Tenth Annual International Workshop on Magnetic Resonance Angiography, Park City, Utah, Sept 29–Oct 3, 1998.
30. Essig M, Reichenbach JR, Schad LR, et al. High-resolution MR venography of cerebral arteriovenous malformations. *Magn Reson Imaging* 1999;17:1417–25.
31. Lee BCP, Vo KD, Kido DK, et al. MR high-resolution blood oxygenation level-dependent venography of occult (low-flow) vascular lesions. *AJNR* 1999;20:1239–42.
32. Liauw L, van Buchem MA, Spilt A, et al. MR angiography of the intracranial venous system. *Radiology* 2000;214:678–82.
33. Chakeres DW, Schmalbrock P, Brogan M, et al. Normal venous anatomy of the brain: demonstration with gadopentetate dimeglumine in enhanced three-dimensional MR angiography. *AJR* 1991; 156:161–72.
34. Creasy JL, Price RR, Prebrey T, et al. Gadolinium-enhanced MR angiography. *Radiology* 1990;175:280–3.
35. Lin W, Mukherjee P, An H, et al. Improving high-resolution MR BOLD venography imaging using a T1 reducing contrast agent. *J Magn Reson Imaging* 1999;10:118–23.
36. Ogawa S, Lee T. Magnetic resonance imaging of blood vessels at high fields: in vivo and in-vitro measurements and image simulations. *Magn Reson Med* 1990;16:9–18.
37. Reichenbach JR, Venkatesan R, Yablonskiy DA, et al. Theory and application of static field inhomogeneity effects in gradient-echo imaging. *J Magn Reson Imaging* 1997;7:266–79.
38. Yang QX, Dardzinski BJ, Li S, et al. Multi-gradient echo with susceptibility inhomogeneity compensation (MGESIC): demonstration of fMRI in the olfactory cortex at 3.0 T. *Magn Reson Med* 1997;37:331–5.
39. Wansapura JP, Holland SK, Dunn RS, et al. NMR relaxation times in the human brain at 3.0 Tesla. *J Magn Reson Imaging* 1999;9:531–8.
40. Hoult DI, Lauterbur PC. The sensitivity of the zeugmatographic experiment involving human samples. *J Magn Res* 1979;34: 425–33.
41. Edelstein WA, Glover GH, Hardy CJ, et al. The intrinsic signal-to-noise ratio in NMR imaging. *Magn Reson Med* 1986;3:604–18.
42. Christoforidis GA, Bourekas EC, Baujan M, et al. High resolution MRI of the deep brain vascular anatomy at 8 Tesla: susceptibility-based enhancement of the venous structures. *J Comput Assis Tomogr* 1999;23:857–66.